

RSC Publishing PCCP

**Selective TDDFT with Automatic Removal of Ghost  
Transitions: Application to a Perylene-Dye-Sensitized Solar  
Cell Model**

Journal:	<i>Physical Chemistry Chemical Physics</i>
Manuscript ID:	Draft
Article Type:	Paper
Date Submitted by the Author:	n/a
Complete List of Authors:	Kovyshin, Arseny; Technische Universitaet Braunschweig, Institut fuer Physikalische und Theoretische Chemie De Angelis, Filippo; Universita di Perugia, Istituto CNR di Scienze e Tecnologie Molecolari (ISTIM-CNR), c/o Dipartimento di Chimica Neugebauer, Johannes; Technische Universitaet Braunschweig, Institut fuer Physikalische und Theoretische Chemie

SCHOLARONE™  
Manuscripts

# Selective TDDFT with Automatic Removal of Ghost Transitions: Application to a Perylene-Dye-Sensitized Solar Cell Model

Arseny Kovyrshin<sup>†‡</sup>, Filippo De Angelis<sup>⊥</sup>, and Johannes Neugebauer<sup>†1</sup>

<sup>†</sup> Technical University Braunschweig, Institute for Physical and Theoretical Chemistry,  
Hans-Sommer-Strasse 10, 38106 Braunschweig, Germany

<sup>‡</sup> Gorlaeus Laboratories, Leiden Institute of Chemistry, Leiden University,  
P.O. Box 9502, 2300 RA Leiden, The Netherlands

<sup>⊥</sup> Istituto CNR di Scienze e Tecnologie Molecolari (ISTIM-CNR), c/o Dipartimento di  
Chimica, Università di Perugia,  
Via elce di Sotto 8, I-06213 Perugia, Italy

Date: March 16, 2012

Status: submitted to *Phys. Chem. Chem. Phys.*

---

<sup>1</sup>Email: j.neugebauer@tu-braunschweig.de

## Abstract

We present an application of a selective time-dependent density-functional theory (TDDFT) scheme to a model for a dye-sensitized solar cell (DSSC) with a perylene sensitizer dye on a  $\text{TiO}_2$  nanoparticle model. In an earlier study on this system [*Chem. Phys. Lett.* **493** (2010), 323], it was reported that a large number of conduction-band excitations severely complicate the identification of the bright  $\pi \longrightarrow \pi^*$  excitations of the perylene dye. Here, we show that this problem can be overcome by applying a selective TDDFT solver based on a guess for the relevant orbital transition in combination with a suitable root-homing scheme. In order to enhance the efficiency of this algorithm we implement an automatic removal scheme for artificially low-lying long-range charge-transfer transitions from the TDDFT eigenvalue problem. A large number of such transitions appears in explicitly solvated systems in the form of inter-solvent or solvent-solute transitions. We study the characteristics of this removal scheme for a small water cluster and then apply it in a TDDFT calculation to a perylene- $\text{TiO}_2$  nanoparticle model system and to perylene explicitly solvated in methanol.

# 1 Introduction

Since the publication of the seminal paper by O'Regan and Grätzel [1], dye-sensitized solar cells (DSSCs) have attracted an ever-increasing attention as possible low-cost alternatives to silicon-based solar cells. For a long time, Ru(II)-polypyridyl dyes reaching efficiencies larger than 11 % have been considered the most successful sensitizer dyes for TiO<sub>2</sub> based DSSCs (for reviews, see Refs. [2–5]). Recently, however, a strategy based on Zn-porphyrins with a Cobalt (II/III) redox couple was reported to show an efficiency exceeding 12 % [6]. This is an important step, as it avoids the limitations of the standard iodide/triiodide redox couple and the use of expensive metals such as ruthenium. Further efficiency improvements can be expected from optimizing the properties of the sensitizing dyes, in particular their energy gap [7,8].

As a completely metal-free alternative to the widely used class of ruthenium (II) complexes, perylene dyes have demonstrated good efficiency in solid-state devices [9] and in liquid electrolyte DSSCs [10]. Theoretical studies have played an important role in understanding the electronic properties of such sensitizer dyes and in predicting organic molecules with optimized properties for DSSCs. Access to information about properties of DSSCs before fabrication can be a great advantage, since a purely combinatorial experimental approach is not practical. Le Bahers et. al. [11] proposed a theoretical protocol for the step-by-step design of DSSCs. The effect of anchoring and spacer groups in perylene sensitizer dyes on the binding properties to a TiO<sub>2</sub> surface or nanocrystal and on the electron injection mechanism was studied in Refs. [12,13]. The optical properties of and heterointerfaces in squaraine-based DSSCs have been studied in Refs. [14,15]. Calculated energies of the highest occupied (HOMO) and lowest unoccupied molecular orbital (LUMO) are frequently used as simple indicators for electron-transfer properties of the dyes [16–18].

Recently, the electron-injection mechanism has been studied for perylene dyes on a  $\text{TiO}_2$  nanoparticle model [18, 19]. While a non-conjugated anchoring group led to a weak electronic coupling and an indirect injection mechanism, a stronger electronic coupling and thus a partially direct electron injection mechanism was suggested for a dye with a conjugated anchoring group. The stronger electronic coupling for the second dye became apparent in a rather large red-shift in the calculated absorption maximum when compared to solution (2.43 eV compared to 2.17 eV), while the absorption maximum hardly changed for the first dye upon adsorption (2.73 eV adsorbed compared to 2.79 in solution). This study thus underlines that it is in general not sufficient to investigate the excited-state properties of the isolated dye molecule. Instead, it is necessary to consider the adsorption explicitly in theoretical studies, since the effect on the properties of the dye can be very different depending on the linker group.

This requirement poses a great challenge to the arsenal of currently available quantum-chemical methods for excited states. The size of combined dye- $\text{TiO}_2$ -nanoparticle models is typically beyond the feasibility of reliable wavefunction-based methods for excited states, so that TDDFT is the workhorse in applications of this type. As has been demonstrated in Ref. [18], the energetic position of the low-lying dye excited states is problematic, as it may fall into a manifold of  $\text{TiO}_2$  conduction-band states. In typical TDDFT solution schemes, the excited-state energies are obtained as solutions of a large matrix eigenvalue problem and are calculated in order of increasing energy. If many conduction-band states appear in the same energy region or below the interesting dye excitation, the computational effort increases tremendously, since all lower-lying states need to be calculated first. An alternative procedure was proposed in Refs. [20, 21], and employed in a study on a DSSC system in Ref. [14]. This procedure avoids the matrix diagonalization, at the price of losing the eigenvector information for the excited states, thus making an assignment of bands in the spectrum much harder.

The problem is expected to become even worse if the solvent shall be studied explicitly, instead of an implicit description used in many theoretical studies. The system size is further increased, and additional low-lying electronic states may appear if (computationally cheap) non-hybrid exchange–correlation functionals or functionals with a low percentage of exact exchange are used [22–27]. Most of these states, which are sometimes called “ghost states” [28], are of long-range charge-transfer (CT) type, and can severely hamper the identification of the relevant excitations [23].

For similarly problematic cases, we have recently developed and successfully tested a selective Davidson diagonalization algorithm in the context of TDDFT [29,30], which allows to predefine the excitation to be calculated in terms of the dominant orbital transitions. The calculation of lower-lying excitations is avoided, but the eigenvector information for the targeted transition is fully preserved (similar to analogous schemes for vibrational problems [31,32]). Based on this reasoning, it can be expected that applications to DSSC model systems like the ones in Ref. [18] should gain a major benefit from such a selective TDDFT scheme, thus opening an elegant route towards more efficient theoretical studies of new dyes in DSSC applications. In particular for organic dyes like the perylene-type molecules studied in Ref. [18] the relevant excited states in the DSSC model systems are dominated by HOMO (highest occupied molecular orbital) to LUMO (lowest unoccupied molecular orbital) orbital transitions, so that guess transitions needed in the selective optimization schemes are readily obtained. It can even be speculated that calculations on systems with indirect injection mechanisms will converge faster than those with direct injection mechanisms due to strong interactions between dye and nanoparticle model, so that the early stages of the optimization may allow preliminary conclusions on the type of mechanism.

In this work, we will provide a pilot application of the state-selective TDDFT algorithm to DSSC model systems. Since especially studies with explicit solvation and non-hybrid

functionals are causing problems, we will test further algorithmic improvements. In particular, we present an implementation that automatically identifies long-range charge-transfer orbital pairs in the calculation by using an orbital-density based overlap criterion suggested in Ref. [25], and then removes the long-range charge-transfer pairs (corresponding to “ghost states”) from the basis in which the TDDFT matrix eigenvalue problem is solved. We analyze the error introduced into the excitation energies by this procedure.

This work is organized as follows: In Sec. 2, the underlying theoretical background will briefly be repeated, and the automatic procedure for neglecting long-range charge-transfer orbital transitions in the TDDFT eigenvalue problem will be discussed. Computational details are given in Sec. 3, before we present a technical test of the CT removal scheme on a small water cluster in Sec. 4. In Sec. 5, we apply our method to a prototypical organic sensitizer dye of perylene type, and study the effect of explicit solvation and of a TiO<sub>2</sub> nanoparticle model, before we conclude from our results in Sec. 7.

## 2 Theory

TDDFT excitation energies for non-hybrid functionals can be obtained by solving the symmetric eigenvalue problem [33–35],

$$[\mathbf{\Omega} - \omega_k^2 \mathbf{1}] \mathbf{F}_k = \mathbf{0}, \quad (1)$$

where the eigenvectors  $\mathbf{F}_k$  describe the character of the excitation in terms of orbital transitions and  $\hbar\omega_k$  is the excitation energy. The elements of the symmetric matrix  $\mathbf{\Omega}$  can be expressed in terms of the coupling matrix  $\mathbf{K}$  through the expression,

$$\Omega_{jb,ia} = \delta_{ab}\delta_{ij}\omega_{jb}^2 + 2\sqrt{\omega_{jb}}K_{jb,ia}\sqrt{\omega_{ia}}. \quad (2)$$

Here,  $\omega_{jb} = \epsilon_b - \epsilon_j$  is the difference between the corresponding virtual and occupied Kohn-Sham orbital energies. The labels  $i, j, \dots$  are used for occupied orbitals and the

labels  $a, b, \dots$  for virtual orbitals here and in the following. The coupling matrix  $\mathbf{K}$  is given as,

$$\mathbf{K}_{ia,jb} = \iint \psi_i(\mathbf{x}_1) \psi_a(\mathbf{x}_1) \left( \frac{1}{r_{12}} + f_{XC} \right) \psi_j(\mathbf{x}_2) \psi_b(\mathbf{x}_2) d\mathbf{x}_1 d\mathbf{x}_2, \quad (3)$$

where  $\psi_s$  are the Kohn–Sham orbitals and  $f_{XC}$  is the exchange–correlation kernel.

Eq. (1) is typically solved by iterative schemes which start with guess vectors  $\mathbf{F}_k^{(0)}$  for the  $N$  lowest excitations. When evaluating the matrix–vector products in Eq. (1) with such an approximation, we get,

$$[\mathbf{\Omega} - \lambda_k^2 \mathbf{1}] \mathbf{F}_k^{(0)} = \mathbf{r}, \quad (4)$$

where  $\lambda_k^2$  is an approximate eigenvalue, and  $\mathbf{r}$  is a residual vector. This vector can be used to construct a correction vector  $\delta_k$  for  $\mathbf{F}_k^{(0)}$  by requiring that

$$[\mathbf{\Omega} - \lambda_k^2 \mathbf{1}] (\mathbf{F}_k^{(0)} + \delta_k) = \mathbf{0}, \quad (5)$$

or

$$\delta_k = -(\mathbf{\Omega} - \lambda_k^2 \mathbf{I})^{-1} (\mathbf{\Omega} - \lambda_k^2 \mathbf{I}) \mathbf{F}_k = -(\mathbf{\Omega} - \lambda_k^2 \mathbf{I})^{-1} \mathbf{r}. \quad (6)$$

In this equation, an approximation for  $\mathbf{\Omega}$  in the inverse is used, usually the dominant contribution to the diagonal, namely, the squared orbital energy differences. This procedure is repeated iteratively, and in each iteration one new basis vector is created for each approximate solution vector to be improved. With this growing basis, more and more approximate eigenvectors are obtained in the following iterations. In the simplest case, the lowest-energy solutions are chosen for further optimization, which can lead to the problems described in Ref. [18], e.g., if many conduction-band states appear below the sought-for valence excitation. In our recent work [29, 30], we have shown how a selective optimization of higher-lying excited states can be achieved by combining suitable guess vectors with root-homing techniques to identify the relevant excitations among the (possibly large number of) approximate solution vectors.



One reason for the appearance of many solution vectors at low energy in TDDFT calculations employing cost-effective (semi-)local exchange–correlation (XC) functionals and the corresponding XC potentials and kernels is the underestimation of long-range charge-transfer (CT) excitation energies by these functionals. In particular, the differential overlap between a long-range CT orbital pair  $\psi_l, \psi_c$  is zero, so that all coupling matrix elements  $K_{lc,jb}$  for this pair will vanish for (semi-)local kernels  $f_{XC}$  [22, 24–27, 36]. Thus, the excitation energy obtained for such a pair will be,

$$E_{CT}^{TDDFT} \approx \omega_{lc} = \epsilon_c - \epsilon_l, \quad (7)$$

whereas the true CT excitation energy is approximately,

$$E_{CT} \approx I^D - A^A - \frac{1}{R}, \quad (8)$$

where  $I^D$  and  $A^A$  are vertical ionization energy of the donor and electron affinity of the acceptor, respectively, and  $R$  is the distance between the donor and acceptor. Besides the lack of the asymptotic  $1/R$  term, the Kohn–Sham virtual-orbital energy  $\epsilon_c$  does not correspond to an electron affinity of the system on which the accepting orbital  $\psi_c$  is located [25, 37]. These two aspects are the main source of a failure of TDDFT in the Adiabatic Local Density Approximation (ALDA) and Adiabatic Generalized Gradient Approximations (AGGA), which lead to the appearance of many artificially low-lying excitations in extended systems (“ghost states” [28]).

The off-diagonal elements of  $\mathbf{\Omega}$  corresponding to long-range CT transitions are

$$\Omega_{lc,ia} = 2\sqrt{\omega_{lc}} \iint \psi_l(\mathbf{x}_1) \psi_c(\mathbf{x}_1) \left( \frac{1}{r_{12}} + f_{XC} \right) \psi_i(\mathbf{x}_2) \psi_a(\mathbf{x}_2) d\mathbf{x}_1 d\mathbf{x}_2 \sqrt{\omega_{ia}}. \quad (9)$$

Since the differential overlap between long-range separated orbitals is nearly zero, these elements have negligible values. Hence, long-range CT orbital transitions do not couple with other orbital pairs for (semi-)local kernels, and it should be possible to exclude them from the eigenvalue problem, Eq. (1), without loss of accuracy for non-CT excitations.

We implemented a computational scheme that automatically removes long-range CT pairs from the matrix  $\mathbf{\Omega}$ . As criteria for the identification of such a long-range CT pair, one can use integrals of the form,

$$C_{ia} = \langle \psi_i^2(x) | \psi_a^2(x) \rangle, \quad (10)$$

as suggested in Ref. [25] and implemented and employed in Refs. [24,38], or the alternative

$$\tilde{C}_{ia} = \langle |\psi_i(x)| | |\psi_j(x)| \rangle \quad (11)$$

that has been used in Ref. [36] as a measure for the long-range CT character of an electronic excitation (and thus as a measure for the reliability of the corresponding TDDFT excitation energy) in terms of the parameter  $\Lambda$ ,

$$\Lambda = \frac{\sum_{ia} \kappa_{ia}^2 \tilde{C}_{ia}}{\sum_{ia} \kappa_{ia}^2}, \quad (12)$$

where  $\kappa_{ia}^2$  is the contribution weight of a certain orbital transition to the entire electronic excitation. In the limit of a long-range charge transfer with no differential spatial overlap of the orbitals  $c$  and  $l$ , the CT orbital pair does not couple to any other orbital pair for (semi)local functionals, so that  $\kappa_{cl}^2 \approx 1$  (unless there are accidental degeneracies) and,

$$\Lambda \approx \tilde{C}_{cl}. \quad (13)$$

A main difference between the work in Refs. [24,25] and the one in Ref. [36] is thus that the  $\Lambda$  parameter of the latter paper was mainly intended as an *a posteriori* diagnostic for a possible CT character of an electronic transition (the contributions  $\kappa_{ia}^2$  are *results* of a linear-response TDDFT calculation). In contrast to that, the quantity  $C_{ia}$  from Ref. [25] was intended as a pre-calculated diagnostic tool to identify long-range CT orbital pairs for which a correction may be applied in the TDDFT calculation *beforehand*. Ref. [24] also mentions the alternative idea of simply removing those rows and columns from  $\mathbf{\Omega}$  which contain at least one long-range CT pair. This of course can only be applied if one

intends to study excitations which are not of long-range CT type, as is the case here. Such a procedure will have the following effects:

- it will reduce the effective size of  $\Omega$  and thus of the eigenvectors and residuals that need to be stored during the iterative diagonalization of the matrix
- it will reduce the computational cost of the matrix vector products  $\Omega \cdot \mathbf{F}$
- it will make the analysis easier, as no (or at least much less) artificially low-lying CT excitations will occur
- it will, however, not affect the non-long-range CT transitions, provided that the threshold for neglecting an orbital pair is chosen in a suitable way.

We would also like to mention that a similar effect is obtained in subsystem-based TDDFT schemes, in which inter-subsystem CT transitions can be avoided by construction [23]. However, subsystem-based schemes may be unsuitable if the interaction strength between the subsystems becomes too large [39].

In this work, we use the quantity  $C_{ia}$  in such a way that orbital pairs are excluded from  $\Omega$  right from the beginning if  $C_{ia}$  is smaller than a predefined threshold. An analysis of suitable values for this threshold is carried out in the following sections. How large the computational savings from neglecting long-range CT orbital pairs really are depends on the particular system type studied. A brief analysis will be presented in Sec. 4.

### 3 Computational details

Structure optimizations for the solvated perylene dye and the perylene dye in Sec. 6 were performed with TURBOMOLE version 6.0 [40,41], using the Perdew-Burke-Ernzerhof (PBE) exchange–correlation (XC) functional [42] together with a split valence polarized

(SVP) basis set from the TURBOMOLE basis set library [43,44]. All other DFT calculations are carried out with the Amsterdam Density Functional (ADF) package [45, 46]. For electronic excitations, a locally modified version [29] of ADF has been applied if not mentioned otherwise.

We employed the PBE XC functional [42] and Becke’s 3-parameter hybrid functional (B3LYP) [47] in combination with double- $\zeta$  polarized (DZP) Slater-type (for oxygen, carbon, and hydrogen atoms) and triple- $\zeta$  polarized (TZP) Slater-type (for titanium atoms) basis sets from the ADF basis set library [45]. The ”Statistical Averaging of Orbital (Model) Potentials” (SAOP) [48] potential and B3LYP in combination with DZP, TZP, and quadruple- $\zeta$  basis set with 4 sets of polarization functions (QZ4P) from the ADF basis set library [45] were used for the test calculations on the perylene molecule.

In calculations with implicit solvent models, we used the Conductor-like Screening Model (COSMO) [49]. Methanol was chosen as a solvent in this model with a dielectric constant of 32.6. A Delly surface [50] was employed for COSMO. Induced electronic charges in the TDDFT calculations influence the COSMO surface charges. For estimation of this effect (”fast solvent response”), we employed the COSMO non-equilibrium solvation model (denoted as ”COSMO response” or CSMRSP below). The desired excitations appear in the region of 400 to 500 nm. The refractive index of methanol in this wavelength regime is approximately 1.33. The non-equilibrium dielectric constant ( $\epsilon_{\text{n.e.}}$ ) as needed for CSMRSP was estimated from the refractive index,  $n$ , using the relationship [51]

$$n = \epsilon_{\text{n.e.}}^{1/2}. \quad (14)$$

The value of the dielectric constant is thus estimated to be 1.8. That value was employed for the non-equilibrium solvation part in ”COSMO response” calculations.

## 4 Technical test: Removal of CT transitions for small water clusters

To study the appearance of long-range CT transitions and to test the validity of the CT removal algorithm proposed in Sec. 2 we first investigate a water dimer as a test system. The structure of the dimer was optimized with PBE/TZP using ADF. The hydrogen-bond length between the two molecules is 1.915 Å. To analyze the dependence of the number of orbital transitions classified as long-range CT on the intermolecular distance, 60 displaced structures were produced by shifting one of the water molecules along the hydrogen bond (with a step size of 0.5 Å). The type of displacement and the equilibrium structure are depicted in Fig. 1.

[Figure 1 about here.]

The total number of occupied-virtual orbital transitions in this system with the TZP basis is 520. 5 different thresholds (from  $10^{-8}$  to  $10^{-4}$  a.u.) for identifying long-range CT orbital transitions were used. The dependence of the number of orbital transitions included in the construction of  $\Omega$  (i.e. non-CT transitions) on the intermolecular distance is shown in Fig. 2 a) for each threshold. At small intermolecular distances, both intra- and intermolecular transitions have relatively high values of the integrals  $\langle \psi_i^2(x) | \psi_a^2(x) \rangle$ , except for transitions with very diffuse Rydberg-type orbitals. This is partially due to the fact that the molecular orbitals of the dimer may be delocalized over both monomers. Therefore, only a few transitions are excluded at small distances, especially if tight thresholds are used. But with increasing intermolecular distance, there are more and more orbital pairs for which  $\langle \psi_i^2(x) | \psi_j^2(x) \rangle$  drops-below the threshold. For distances larger than 18.5 Å between the water molecules, all integrals  $C_{ia}$  are independent of the intermolecular distance. At that point, essentially all intermolecular orbital transitions have been identified as long-range CT transitions with all thresholds tested here.

[Figure 2 about here.]

The number of intramolecular orbital transitions for a system of identical monomers is  $n_{\text{monomers}} \cdot (n_{\text{occ}}^{\text{monomer}} \cdot n_{\text{virt}}^{\text{monomer}})$ , where  $n_{\text{monomers}}$  is a number of monomers,  $n_{\text{occ}}^{\text{monomer}}$  is a number of occupied orbitals on each monomer, and  $n_{\text{virt}}^{\text{monomer}}$  is a number of virtual orbitals on each monomer. The total number of orbital transitions is  $(n_{\text{occ}}^{\text{monomer}} \cdot n_{\text{monomers}}) \cdot (n_{\text{virt}}^{\text{monomer}} \cdot n_{\text{monomers}})$ . Exclusion of all inter-molecular transitions in the limit of long distance should thus lead to an asymptotic saving of a factor of  $n_{\text{monomers}}$  in the number of orbital transitions to be considered. In fact, the number of transitions at large distances in the dimer is  $520/2 = 260$ .

To study the effect of removing long-range CT transitions on excitation energies of non-CT transitions, the  $n \rightarrow 3p$  orbital transition localized on one of the water molecules in the dimer was chosen. The orbitals involved in this transition are shown in the inset in Fig. 2 d). The dependence of the targeted excitation energy on the CT threshold for the equilibrium structure of the dimer is shown in Fig. 2 b). As can be seen from that plot, neither the number of transitions nor the excitation energy change much with the CT threshold. Deviations are seen only at rather high values for the CT threshold, where already some of the localized transitions are removed. When the monomers are displaced by 10 Å from the equilibrium distance, the energy does not change significantly until the CT threshold is equal to  $5 \times 10^{-3}$  a.u., see Fig. 2 c). But the number of orbital transitions included in the construction of  $\Omega$  decreases very fast with the change of the threshold: more than half of the transitions can be removed with an error smaller than 0.0003 eV. At a displacement of 20 Å (or larger) from the equilibrium, the excitation energy and the number of orbital transitions do not depend much on the CT threshold, similar to the case of the equilibrium structure, see Fig. 2 d). But in this case, starting from the lowest CT threshold the number of orbital transitions in the construction of  $\Omega$  is equal to half of the total number one. This means that only intramolecular orbital transitions

are considered as non-CT orbital transitions even with very low thresholds.

We also tested this CT removal scheme for a case with more subunits, namely, a water tetramer (not shown). As expected, the behavior is very similar to the dimer case: The number of orbital transitions considered at the equilibrium structure (TZP basis) is 2080, and in the limit of long range it is  $2080/4 = 520$ , thus nicely illustrating the potential savings brought about by the method.

## 5 Excited states of perylene dyes in DSSC model systems

In this section, we are going to study whether the selective TDDFT solver together with the removal of ghost transitions offers advantages in the determination of excitation energies of sensitizer dyes in DSSC models. In particular, we will address the question whether advantages arise in studies that explicitly consider the molecular environment, e.g., the solute or the support on which the dye is adsorbed. Two types of perylene dyes will be studied, a perylene dye with a non-conjugated space-anchoring group [dye I, see inset in Fig. 3 a)] and a perylene dye with a conjugated space anchoring group (dye II, see inset in Fig. 6). We will focus on the important high-intensity excitation dominated by the HOMO→LUMO transition of the perylene dyes. Since our code is currently restricted to non-hybrid functionals and is embedded in the Slater function based ADF code, we will start with a short test of different exchange–correlation functionals and basis sets using conventional TDDFT solvers to make our methodology comparable to earlier data derived from B3LYP/6-31G\* calculations [18]. Then, we will compare our selective TDDFT solver to the conventional calculation of TDDFT excitation energies for dye I. These tests concerns the isolated molecule, the molecule in solution, and the molecule adsorbed to a TiO<sub>2</sub> nanoparticle model. In the latter cases, we are also going to investigate

the effect of the automatic removal of ghost transitions. Finally, we will extend our study to dye II and compare the results obtained for this molecule to the ones for dye I.

The structure of the perylene dye I and the dye adsorbed on a  $\text{TiO}_2$  nanoparticle model were taken from Ref. [18]. They are shown in Fig. 3 a).

[Figure 3 about here.]

## 5.1 Isolated perylene dye I

The HOMO  $\rightarrow$  LUMO transition of perylene dye I has been analyzed in Ref. [18] using B3LYP. Since our selective TDDFT solver currently is not yet capable of using hybrid functionals, we studied the excitation energy for this transition with three different exchange–correlation potentials for the isolated dye, making use of the standard TDDFT solver in ADF. The isosurface plots of the orbitals involved into the dominant orbital transition are depicted in the insets in Fig. 4 a). The results obtained with PBE, SAOP, and B3LYP with different basis sets are shown in Table I. B3LYP/6-31G\* data without solvent model obtained were calculated with TURBOMOLE version 6.0 [40,41].

[Table 1 about here.]

From the values in Table II we see that the PBE and SAOP results agree within 0.01 eV. The change from a DZ to a DZP basis set is quite pronounced ( $\sim 0.11$  eV), while a further increase to a TZP or QZ4P basis leads to smaller changes. The B3LYP results are slightly more affected by increasing the basis, but overall there is a rather systematic shift of 0.23 to 0.25 eV between the PBE and B3LYP results (0.22 and 0.24 eV between SAOP and B3LYP; not recognizable from the data in Table I due to round-off effects). In view of the system sizes to be studied in the following, we chose the DZP basis for further calculations as a good compromise between accuracy and efficiency.



## 5.2 Solvation effects and test of the selective TDDFT solver

A typical solvent used in DSSCs is methanol. Therefore, the C-PCM solvation model [52] has been used in in Ref. [18] to study the HOMO  $\rightarrow$  LUMO transition of the perylene dyes. The resulting excitation energy (B3LYP/6-31G\*) was 2.79 eV. A B3LYP/6-31G\* calculation for the isolated dye yields an excitation energy of 2.87 eV (see Table II), so that the shift induced by the continuum solvation model is  $-0.08$  eV. A B3LYP/DZP calculation with ADF results in an excitation energy of 2.80 eV, and if the solvent is included in terms of a similar dielectric model (COSMO, including the fast solvent response, dubbed CSMRSP here), we also obtain a shift of  $-0.08$  eV. This shows that CSMRSP and C-PCM predict similar shifts in the excitation energy in the present case. The offset of 0.07 eV between the B3LYP/6-31G\* and the B3LYP/DZP calculations is mainly attributed to the different basis sets employed (it should be kept in mind that DZP is a Slater-type basis set). The experimental excitation energy in methanol is 2.81 eV [53].

A PBE/DZP calculation using the conventional TDDFT solver in ADF results in an excitation energy of 2.56 eV and a HOMO  $\rightarrow$  LUMO contribution weight of 96.2 %. If the COSMO model is included only for the ground-state polarization (no fast solvent response), the excitation energy increases by 0.02 eV, while the HOMO  $\rightarrow$  LUMO contribution weight stays the same. These results are perfectly reproduced by the selective TDDFT solver, which converges nicely in 8 iterations in both cases. If also the fast solvent response is included (CSMRSP; currently only possible with the standard solver), the excitation energy decreases by 0.07 eV compared to the isolated molecule, which is in nice agreement with the B3LYP-based shifts.

A drawback of continuum solvation models is that specific solvation effects cannot be covered. A major advantage, however, is that no configurational averaging over different solvent-solute snapshots is necessary, as this is effectively included in the parameterization of the model. Considering solvent effects in more detail requires to have a fast method at

hand for the calculation of explicitly solvated structures of the dye. Here, we are going to test this for a structure of perylene dye I solvated by 42 methanol molecules. The structure of the solvent shell was optimized (PBE/SVP) using the TURBOMOLE program package, while keeping the coordinates of the perylene dye frozen (coordinates taken from Ref. [18]). In this way, only electronic effects are evaluated. The resulting structure is shown in Fig. 3 b).

We calculated the excitation energies of this system with PBE/DZP. The excitation corresponding to the HOMO→LUMO transition for perylene was identified on the basis of isosurface plots of the Kohn–Sham orbitals from the solvated system, which were compared to those of the isolated system. The HOMO→LUMO transition of the perylene subunit in the solvated model also corresponds to the HOMO→LUMO transition of the whole system. The presence of the methanol molecules thus does not lead to any orbital transitions with orbital-energy differences lower than that of the targeted one. The orbitals involved in the transition under study are almost completely localized on the perylene molecule, with hardly any contribution from the solvent molecules [see Fig. 4 a)]. Although this system contains a rather large number of atoms (293), it is not problematic to find the desired excitation with a standard TDDFT solver. In a PBE/DZP calculation on the lowest 50 excited states of the system, the excitation energy decreased to the value of 2.48 eV (compared to 2.56 eV for the free perylene dye) under the influence of the solvent molecules, and changed position in the spectrum from the lowest-energy to the fourth excitation. This change is due to the presence of ghost transitions of long-range CT type, which are dominated by transitions from orbitals of the solvent molecules to the LUMO of the dye. The contribution of the HOMO → LUMO transition to the identified excitation is lower than in the isolated case and amounts to only 88.4 %. The selective Davidson calculation is in perfect agreement with the reference results, leading to an excitation energy of 2.48 eV with a contribution of the HOMO → LUMO transition equal to 88.5 %. Convergence was easily achieved within 7 iterations. The computational effort

is thus much lower than in the standard calculation (7 matrix–vector products of the TDDFT response matrix with basis vectors compared to 530 in the case of the standard solution), but this comparison is not entirely fair in this case because far too many solution vectors have been calculated with the standard solver. To a certain extent, however, this reflects the uncertainty about the position of a desired excitation at the beginning of each TDDFT calculation on extended systems.

[Figure 4 about here.]

In order to investigate whether the underestimated long-range CT orbital transitions affect the calculation, we employed the automatic removal scheme introduced in Sec. 2. As criteria for the identification of long range CT transitions, thresholds for the integrals  $\langle \psi_i^2(\mathbf{x}) | \psi_a^2(\mathbf{x}) \rangle$  between  $5 \times 10^{-3}$  and  $1 \times 10^{-7}$  have been tested in selective TDDFT calculations. The dependence of the excitation energy on the threshold is shown in Fig. 5 a). About 60000 orbital transitions can be removed from the  $\mathbf{\Omega}$  matrix without significant loss of accuracy ( $<0.005$  eV) using a threshold of  $5 \times 10^{-5}$  a.u. However, compared to the total number of orbital transitions (968596), this corresponds to only a modest reduction of 6.16 % for this system. One can see from Fig. 5 b) that up to 20 % of the orbital transitions may be removed with an acceptable error of 0.04 eV.

[Figure 5 about here.]

Although only a single structure has been investigated here, and the results clearly should not be over-interpreted, we observe that the energy decrease is in line with the result predicted by the COSMO/CSMRSP model in the previous section. Preliminary tests with larger solvation models indicate that explicit inclusion of even more solvent molecules may lead to a further lowering of this value.

### 5.3 Adsorbed perylene dye I

To study the excitation energy of perylene dye I adsorbed on  $\text{TiO}_2$ , the perylene– $\text{TiO}_2$  adsorbate model from Ref. [18] was considered. The same procedure as for the solvated system was employed to find the desired dominant orbital transition of the dye in the nanoparticle model in a PBE/DZP calculation. Isosurface plots of the orbitals are shown in Figure 4 b).

The HOMO of the free dye corresponds to the HOMO of the adsorbed system, and the LUMO of the free dye corresponds to the LUMO+43 of the adsorbate system. A reference calculation (PBE/DZP) of the lowest 150 excitations was performed with a conventional TDDFT solver. The update scheme of the Davidson method was one vector at a time (cf. Ref. [29]). The excitation dominated by the targeted orbital transition was found as excitation number 101 with an energy of 2.51 eV. After constructing the guess vector for the HOMO→LUMO+43 orbital transition in the adsorbed system, the excitation energy was optimized with the selective Davidson algorithm using PBE/DZP/COSMO and PBE/DZP. The final excitation energies are presented in Table II. The excitation energies of reference and selective calculation are in perfect agreement. But there is a deviation in the contribution of the dominant orbital transition. The contribution of the HOMO→LUMO+43 transition in the selective calculation is 86.2 %, whereas it is only 69.6 % in the reference calculation. This can be explained by the update scheme used in the reference calculation, which sometimes leads to less well converged roots, especially in dense regions of the spectrum with many (near-) degeneracies [30], as is the case here. Still, the eigenvalues from this update scheme may be reliable, as eigenvalues converge faster than eigenvectors in Davidson-type methods [54].

Concerning the computational cost, the selective calculation (PBE/DZP) requires 10 matrix–vector products (cf. Refs. [29, 30]), while 180 matrix–vector products are used in the standard solution; a solution with the more robust update scheme “all-at-once” [29],

which typically gives better-converged eigenvectors, would have required many more matrix–vector products, but could not be carried out due to the high memory demands.

[Table 2 about here.]

In Ref. [18], the HOMO→LUMO excitation (B3LYP/6-31G\*, C-PCM) for dye I was compared to the corresponding transition for the adsorbed perylene dye. The calculations result in a shift due to adsorption of  $-0.06$  eV. Our PBE/DZP calculations lead to comparable shifts of  $-0.05$  eV, both with the selective and the standard solution (see Table II). The use of COSMO in the calculation of KS orbitals and orbital energies does not change this difference, though it shifts both excitation energies by  $+0.02$  eV.

As was mentioned in Sec. 1, the presence of the  $\text{TiO}_2$  nanoparticle model may lead to the appearance of low-lying electronic transitions in the eigenvalue spectrum. Therefore, we also carried out a CT analysis for this system. The dependence of the excitation energy on the CT threshold and the dependence of the error in the excitation energy on the percentage of removed orbital transitions are shown in Fig. 5 c), d). The total number of orbital transition is 1923888, of which 137544 can be considered as long-range CT transitions and thus excluded from the  $\mathbf{\Omega}$  matrix using a threshold of  $5 \times 10^{-5}$ . Although this is again only a modest saving, we would like to note that CT-free calculations result in better convergence for the selective Davidson algorithm, which is probably due to less severe root-switching induced by the presence of low-lying long-range CT transitions in the original calculation.

## 6 Adsorbed perylene dye II

To compare the excitation energies of the two different dyes (dye I and II) with their different anchoring groups, we considered a DSSC model with perylene dye II, which

contains a conjugated space-anchoring group. The structure for this model was taken from Ref. [18]; it is shown in Fig. 6.

[Figure 6 about here.]

The orbitals involved in the HOMO $\rightarrow$ LUMO ( $\pi \rightarrow \pi^*$ ) transition of perylene dye II in the DSSC model and in isolated perylene are shown in Fig. 7. The HOMO $\rightarrow$ LUMO orbital transition in isolated perylene corresponds to the HOMO $\rightarrow$ LUMO+4 orbital transition in the DSSC model. The LUMO+4 is energetically close to the TiO<sub>2</sub> conduction band, hence the HOMO $\rightarrow$ LUMO+4 transition mixes with low-lying TiO<sub>2</sub> bulk medium excitations.

[Figure 7 about here.]

The perylene dye with unsaturated spacer-anchoring group shows strong electronic coupling with the unoccupied TiO<sub>2</sub> states in the DSSC model [18]. Such an electronic coupling leads to the presence of orbital transitions from the HOMO on perylene to TiO<sub>2</sub> bulk medium unoccupied orbitals (BM), which are close in energy to the  $\pi \rightarrow \pi^*$  transition on perylene. Hence the  $\pi \rightarrow \pi^*$  orbital transition strongly mixes with near-degenerate HOMO $\rightarrow$ BM transitions. As a result, the convergence behavior of this excitation in our selective calculation (PBE/DZP) is more complicated than the corresponding transition in dye I.

The energy of the excitation with the highest contribution of the HOMO $\rightarrow$ LUMO+4 ( $\pi \rightarrow \pi^*$ ) orbital transition in the adsorbed system is 1.95 eV (see Table III), while the energy of the corresponding excitation in the isolated perylene dye II is 2.17 eV. The relevant energies obtained in Ref. [18] with B3LYP/6-31G\*/C-PCM are 2.17 eV and 2.43 eV. The shift of  $-0.26$  eV induced by adsorption is thus comparable to the one obtained in our calculation ( $-0.22$  eV). Also when comparing the shifts induced by adsorption

for dye I and dye II, we observe a value which is 0.17 eV larger for dye II in our work compared to 0.20 eV in Ref. [18].

[Table 3 about here.]

Starting from the first iterations, the HOMO $\rightarrow$ LUMO+4 transition strongly mixes with HOMO $\rightarrow$ BM transitions, and its contribution to the final excitation is only 15.53 %, which is much lower than and thus qualitatively different from the case of dye I with the saturated space anchoring group (86.2 %). The converged excitation is dominated by HOMO $\rightarrow$ BM transitions. As was already mentioned in Ref. [18], such a mixing of the  $\Pi \rightarrow \Pi^*$  transition with HOMO $\rightarrow$ BM transitions plays an important role in the direct electron injection mechanism in DSSC. In the present case of a non-hybrid functional, however, the HOMO $\rightarrow$ BM-type transitions may be underestimated in energy as they have (partially) long-range charge transfer character. This could lead to an overestimation of mixings and thus to an underestimation of the HOMO $\rightarrow$ LUMO+4 contribution in the final transition. Therefore, we again tested the application of the CT-removal algorithm. The total number of orbital transitions in the system is 1914250. Only 53357 transitions (roughly 3 %) can be removed with a loss in accuracy of less than 0.001 eV (CT threshold is  $10^{-5}$  a.u.). This number is quite small in comparison with dye I. The dependence of the excitation energy on the value of the long-range CT threshold and the dependence of the error in the excitation energy on the percentage of removed orbital transitions is depicted in Fig. 8 b).

[Figure 8 about here.]

It can be seen from the plots that the CT removal algorithm only leads to a small benefit in this case. As a side aspect we note that the resulting orbital composition is sensitive to the CT threshold even if the excitation energy is accurate: Larger thresholds lead to a larger

number of removed CT transitions and thus to a purification of the perylene  $\pi \longrightarrow \pi^*$  transition. This can be seen from Fig. 9 where the contributions of the most important orbital transitions to the excitation under study are presented for CT thresholds which give excitation-energy errors  $< 0.001$  eV.

[Figure 9 about here.]

## 7 Conclusions

In this work, we have presented an application of a selective TDDFT solver to a model for a dye-sensitized solar cell. Our calculations demonstrate that applications of this type, where excited states of adsorbed molecules or molecules in a solvent are under study, benefit significantly from the state-selective solution algorithm. This enables calculations of excited states of the dye molecules with explicit consideration of complicated environments, as present in DSSC models. The comparison with reference results shows that the selective solution scheme gives reliable results for effects on excitation energies induced by such environments.

To further enhance the efficiency of TDDFT calculations on DSSC model systems, we have introduced the possibility to automatically remove orbital pairs of long-distance charge-transfer nature. Such transitions should not have any influence on the remaining transitions in calculations employing non-hybrid XC kernels, and thus can be removed from the TDDFT response matrix. Our tests on small water clusters have shown that this can lead to a dramatic increase in efficiency for systems of several weakly interacting subunits like solvent molecules. However, this effect is less pronounced at short intermolecular distances, especially if orbitals are delocalized over several molecules. The reason for this is that orbital delocalization makes it difficult to find proper thresholds for the overlap integrals of orbital densities, which are used for the definition of a long-range



CT pair. Nevertheless, a reduction of the number of orbital pairs by about 10-20 % with acceptable losses in accuracy can be decisive on whether or not calculations of systems of this type can be carried out. And what is more important, even a slight reduction of the number of orbital transitions can significantly improve the convergence behavior of the selective TDDFT solver.

The HOMO→LUMO orbital transition of dye I in the DSSC model (adsorbed system) appears above a large number of low-energy transitions. This makes it difficult to find with standard TDDFT solvers. The selective solution algorithm offers considerable advantages here due to the simple orbital composition of this excitation. The HOMO→LUMO orbital transition of dye II adsorbed to the TiO<sub>2</sub> nanoparticle model is near-degenerate with bulk orbital transitions of Ti<sub>2</sub>O. This decreases the energy of the excitation in which the HOMO→LUMO orbital transition of dye II is involved. Mixing with orbital transitions to Ti<sub>2</sub>O makes the convergence of the selective TDDFT solver more difficult here, but nevertheless it offers a great advantage, avoiding the calculation of unnecessary states. Overall, the present scheme significantly simplifies the direct calculation of excited states of sensitizer dyes in typical DSSC environments.

## Acknowledgment

This work was supported by a TOP grant of the Netherlands Organization for Scientific Research (NWO) and a computer time grant from the Netherlands National Computing Facilities Foundation (NCF). FDA thanks Fondazione Istituto Italiano di Tecnologia, Platform Computation, Project SEED 2009 “HELYOS” and CNR-EFOR for financial support.

## References

- [1] B. O'Regan and M. Grätzel, *Nature* **353**, 737 (1991).
- [2] A. Hagfeldt and M. Grätzel, *Acc. Chem. Res.* **33**, 269 (2000).
- [3] M. K. Nazeeruddin and M. Grätzel, Conversion and Storage of Solar Energy using Dye-sensitized Nanocrystalline TiO<sub>2</sub> Cells, in *Comprehensive Coordination Chemistry II*, edited by J. A. McCleverty and T. J. Meyer, volume 9, pages 719–758, Elsevier, Amsterdam, 2003.
- [4] M. Grätzel, *Acc. Chem. Res.* **42**, 1788 (2009).
- [5] A. Hagfeldt, G. Boschloo, L. Sun, L. Kloo, and H. Pettersson, *Chem. Rev.* **110**, 6595 (2010).
- [6] A. Yella, H.-W. Lee, H. N. Tsao, C. Yi, A. K. Chandiran, M. Nazeeruddin, and M. Grätzel, *Science* **334**, 629 (2011).
- [7] M. K. Nazeeruddin, F. D. Angelis, S. Fantacci, A. Selloni, G. Viscardi, P. Liska, S. Ito, B. Takeru, and M. Grätzel, *J. Am. Chem. Soc.* **127**, 16835 (2005).
- [8] M. D. McGehee, *Science* **334**, 607 (2011).
- [9] U. B. Cappel, M. H. Karlsson, N. G. Pschirer, F. Eickemeyer, J. Schöneboom, P. Erk, G. Boschloo, and A. Hagfeldt, *J. Phys. Chem. C* **113**, 14595 (2009).
- [10] C. Li, J. Yum, S. Moon, A. Herrmann, F. Eickemeyer, N. G. Pschirer, P. Erk, J. Schöneboom, K. Müllen, M. Grätzel, and M. K. Nazeeruddin, *ChemSusChem* **1**, 615 (2008).
- [11] T. L. Bahers, F. Labat, T. Pauporté, P. P. Lainé, and I. Ciofini, *J. Am. Chem. Soc.* **133**, 8005 (2011).

- [12] M. Nilsing, P. Persson, S. Lunell, and L. Ojamäe, *J. Phys. Chem. C* **111**, 12116 (2007).
- [13] P. Persson, M. J. Lundqvist, R. Ernstorfer, W. A. G. III, and F. Willig, *J. Chem. Theory Comput.* **2**, 441 (2006).
- [14] D. Rocca, R. Gebauer, F. De Angelis, M. K. Nazeeruddin, and S. Baroni, *Chem. Phys. Lett.* **475**, 49 (2009).
- [15] F. D. Angelis, S. Fantacci, and R. Gebauer, *J. Phys. Chem. Lett.* **2**, 813 (2011).
- [16] T. Edvinsson, C. Li, N. Pschirer, J. Schöneboom, F. Eickemeyer, R. Sens, G. Boschloo, A. Herrmann, K. Müllen, and A. Hagfeldt, *J. Phys. Chem. C* **111**, 15137 (2007).
- [17] Z. Ning, Q. Zhang, W. Wu, H. Pei, B. Liu, and H. Tian, *J. Org. Chem.* **73**, 3791 (2008).
- [18] F. De Angelis, *Chem. Phys. Lett.* **493**, 323 (2010).
- [19] J. Li, M. Nilsing, I. Kondov, H. Wang, P. Persson, S. Lunell, and M. Thoss, *J. Phys. Chem. C* **112**, 12326 (2008).
- [20] B. Walker, A. M. Saitta, R. Gebauer, and S. Baroni, *Phys. Rev. Lett.* **96**, 113001 (2006).
- [21] D. Rocca, R. Gebauer, Y. Saad, and S. Baroni, *J. Chem. Phys.* **128**, 154105 (2008).
- [22] J. Autschbach, *ChemPhysChem* **10**, 1757 (2009).
- [23] J. Neugebauer, M. J. Louwerse, E. J. Baerends, and T. A. Wesolowski, *J. Chem. Phys.* **122**, 094115 (2005).
- [24] J. Neugebauer, O. Gritsenko, and E. J. Baerends, *J. Chem. Phys.* **124**, 214102 (2006).

- [25] O. Gritsenko and E. J. Baerends, J. Chem. Phys. **121**, 655 (2004).
- [26] A. Dreuw and M. Head-Gordon, J. Am. Chem. Soc. **126**, 4007 (2004).
- [27] A. Dreuw, J. L. Weisman, and M. Head-Gordon, J. Chem. Phys. **119**, 2943 (2003).
- [28] L. Goerike and S. Grimme, J. Chem. Phys. **132**, 184103 (2010).
- [29] A. Kovyrshin and J. Neugebauer, J. Chem. Phys. **133**, 174114 (2010).
- [30] A. Kovyrshin and J. Neugebauer, Chem. Phys. **391**, 147 (2011).
- [31] M. Reiher and J. Neugebauer, J. Chem. Phys. **118**, 1634 (2003).
- [32] C. Herrmann, J. Neugebauer, and M. Reiher, New J. Chem. **31**, 818 (2007).
- [33] M. E. Casida, Time-Dependent Density Functional Response Theory for Molecules, in *Recent Advances in Density Functional Methods Part I*, edited by D. P. Chong, pages 155–192, World Scientific, Singapore, 1995.
- [34] A. Rosa, G. Ricciardi, O. V. Gritsenko, and E. J. Baerends, Struct. Bonding **112**, 49 (2004).
- [35] J. Neugebauer, Phys. Rep. **489**, 1 (2010).
- [36] M. J. G. Peach, P. Benfield, T. Helgaker, and D. J. Tozer, J. Chem. Phys. **128**, 044118 (2008).
- [37] D. Tozer, J. Chem. Phys. **119**, 12697 (2003).
- [38] J. Neugebauer and E. J. Baerends, J. Phys. Chem. A **110**, 8786 (2006).
- [39] S. Fux, K. Kiewisch, C. R. Jacob, J. Neugebauer, and M. Reiher, Chem. Phys. Lett. **461**, 353 (2008).

- [40] TURBOMOLE V6.0 2009, a development of University of Karlsruhe and Forschungszentrum Karlsruhe GmbH, 1989-2007, TURBOMOLE GmbH, since 2007; available from <http://www.turbomole.com>.
- [41] R. Ahlrichs, M. Bär, M. Häser, H. Horn, and C. Kölmel, Chem. Phys. Lett. **162**, 165 (1989).
- [42] J. P. Perdew, K. Burke, and M. Ernzerhof, Phys. Rev. Lett. **77**, 3865 (1996).
- [43] <ftp://ftp.chemie.uni-karlsruhe.de/pub/jbasen>.
- [44] A. Schäfer, H. Horn, and R. Ahlrichs, J. Chem. Phys. .
- [45] Amsterdam density functional program, Theoretical Chemistry, Vrije Universiteit, Amsterdam, URL: <http://www.scm.com>.
- [46] G. te Velde, F. M. Bickelhaupt, E. J. Baerends, S. J. A. van Gisbergen, C. Fonseca Guerra, J. G. Snijders, and T. Ziegler, J. Comput. Chem. **22**, 931 (2001).
- [47] P. J. Stephens, F. J. Devlin, C. F. Chabalowski, and M. J. Frisch, J. Phys. Chem. **98**, 11623 (1994).
- [48] O. V. Gritsenko, P. R. T. Schipper, and E. J. Baerends, Chem. Phys. Let. **302**, 199 (1999).
- [49] A. Klamt and G. Schüürmann, J. Chem. Soc. Perk. Trans. 2 , 799 (1993).
- [50] B. Delley, Molecular Simulation **32**, 117 (2006).
- [51] P. W. Atkins and R. S. Friedman, *Molecular Quantum Mechanics*, Oxford University Press, Oxford, 3 edition, 1997.
- [52] M. Cossi, N. Rega, G. Scalmani, and V. Barone, J. Comput. Chem. **24**, 669 (2003).

- [53] J. M. Szarko, A. Neubauer, A. Bartelt, L. Socaciu-Siebert, F. Birkner, K. Schwarzburg, T. Hannappel, and R. Eichberger, *J. Phys. Chem. C* **112**, 1054210552 (2008).
- [54] A. Stathopoulos and C. F. Fisher, *Comput. Phys. Commun.* **79**, 268 (1994).

# List of Figures

1	Structure of the water dimer optimized with PBE/TZP. . . . .	31
2	a) Number of orbital transitions included in the construction of $\Omega$ for a water dimer (PBE/TZP) as a function of the intermolecular distance for different long-range CT thresholds (a.u.). Dependence of the $n \rightarrow 3p$ excitation energy on the CT threshold for the b) equilibrium structure; c) 10 Å displacement from equilibrium; d) 20 Å displacement from equilibrium. The inset in d) shows isosurface plots of the $n$ and $3p$ orbitals of a water molecule in a H <sub>2</sub> O dimer (isosurface value: $\pm 0.03$ ). . . . .	32
3	a) Structure of the perylene dye I and the dye I adsorbed on a TiO <sub>2</sub> nanoparticle model (coordinates taken from the work in Ref. [18]), and b) structure of the perylene dye I molecule solvated by 42 methanol molecules optimized with PBE/SVP. . . . .	33
4	Isosurface plots of the HOMO and LUMO of the free perylene dye I [insets of part a)], dye I solvated by 42 methanol molecules [a)], and dye I adsorbed on a TiO <sub>2</sub> nanoparticle model [b)] (isosurface value: $\pm 0.03$ ). . . . .	34
5	a) Dependence of the excitation energy (PBE/DZP) on the value of the CT threshold (a.u.), and b) dependence of the error in the excitation energy on the percentage of removed orbital transitions for the perylene dye I solvated by 42 methanol molecules. c) Dependence of the excitation energy (PBE/DZP) on the value of CT threshold, and d) dependence of error in the excitation energy on the percentage of removed orbital transitions for the perylene dye I adsorbed on TiO <sub>2</sub> nanoparticle model. . . . .	35
6	Structure of perylene dye II and dye II adsorbed on a TiO <sub>2</sub> nanoparticle model (coordinates are taken from Ref. [18]). . . . .	36
7	Isosurface plots of the HOMO and LUMO orbitals of the free perylene dye II and the dye II adsorbed on a TiO <sub>2</sub> nanoparticle model (isosurface value: $\pm 0.03$ ). . . . .	37
8	Dependence of the excitation energy on the value of CT threshold (a.u.) for the perylene dye II adsorbed on the TiO <sub>2</sub> nanoparticle model [a)], and dependence of the error in the excitation energy on the percentage of removed orbital transitions [b)]. . . . .	38
9	Orbital composition of excitation with highest contribution of HOMO $\rightarrow$ LUMO transition of perylene dye II in DSSC for different CT thresholds (a.u.). . .	39

Figure 1: Structure of the water dimer optimized with PBE/TZP.

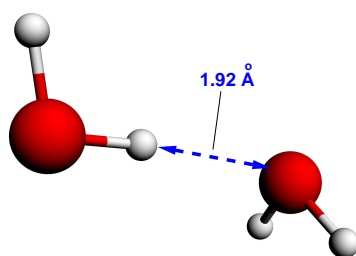




Figure 2: a) Number of orbital transitions included in the construction of  $\Omega$  for a water dimer (PBE/TZP) as a function of the intermolecular distance for different long-range CT thresholds (a.u.). Dependence of the  $n \rightarrow 3p$  excitation energy on the CT threshold for the b) equilibrium structure; c) 10 Å displacement from equilibrium; d) 20 Å displacement from equilibrium. The inset in d) shows isosurface plots of the  $n$  and  $3p$  orbitals of a water molecule in a H<sub>2</sub>O dimer (isosurface value:  $\pm 0.03$ ).

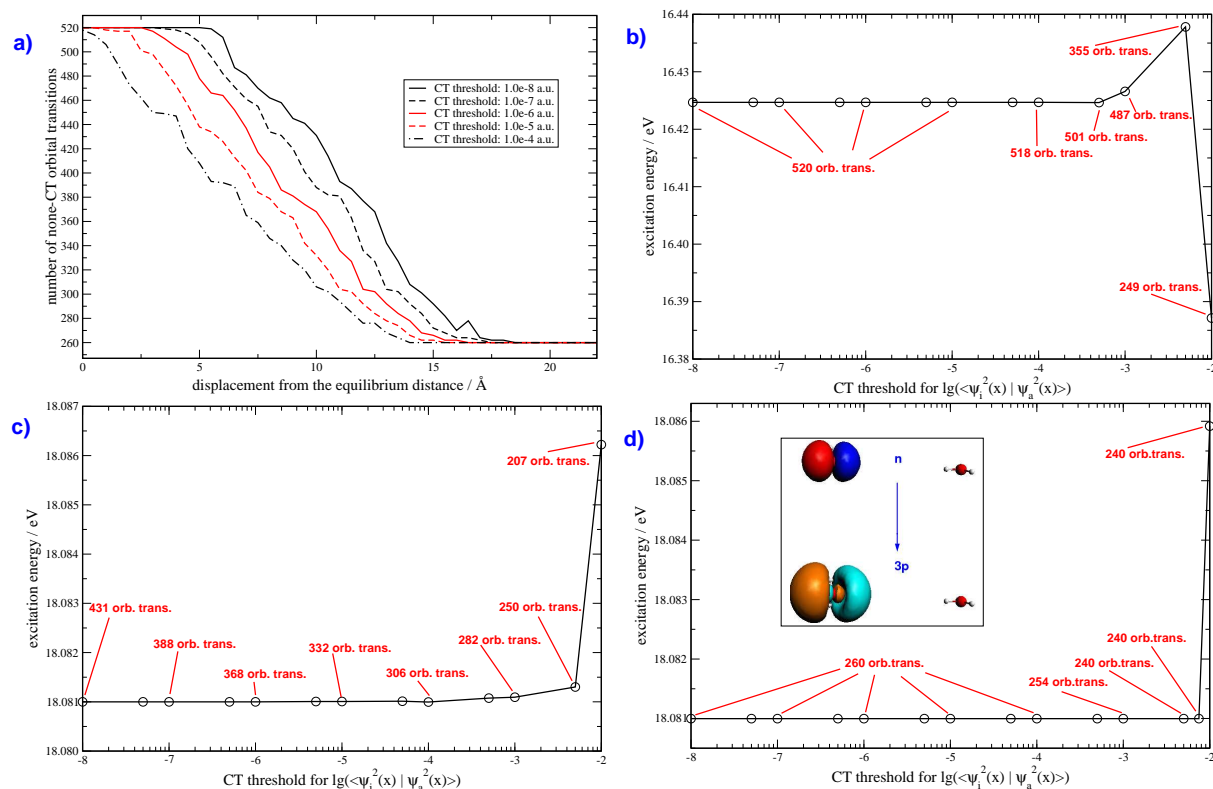


Figure 3: a) Structure of the perylene dye I and the dye I adsorbed on a  $\text{TiO}_2$  nanoparticle model (coordinates taken from the work in Ref. [18]), and b) structure of the perylene dye I molecule solvated by 42 methanol molecules optimized with PBE/SVP.

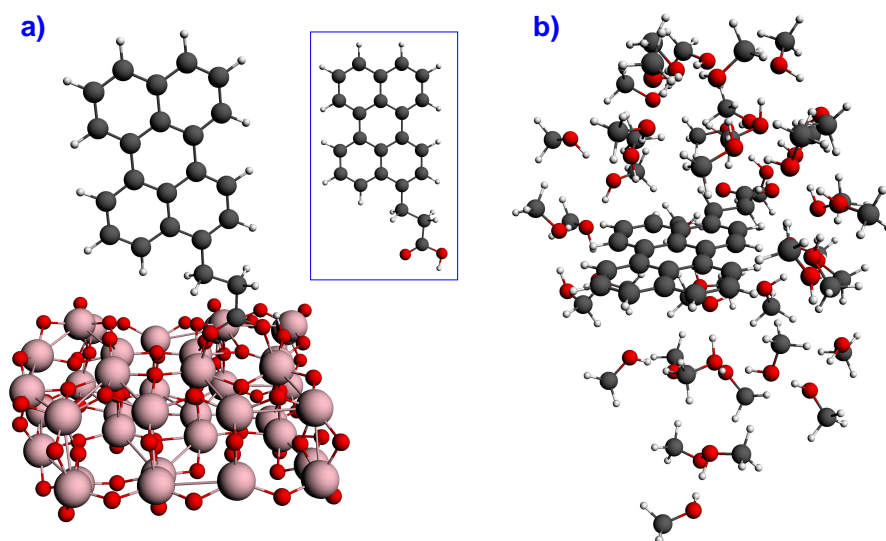


Figure 4: Isosurface plots of the HOMO and LUMO of the free perylene dye I [insets of part a)], dye I solvated by 42 methanol molecules [a)], and dye I adsorbed on a TiO<sub>2</sub> nanoparticle model [b)] (isosurface value:  $\pm 0.03$ ).

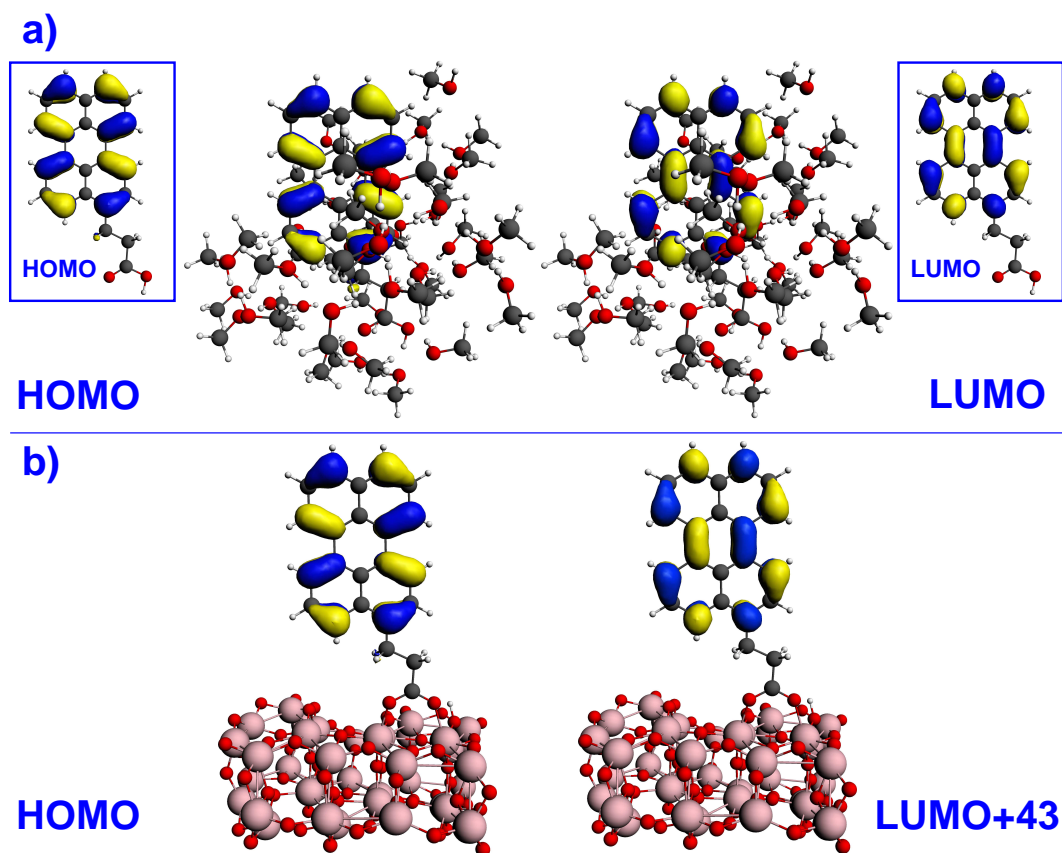


Figure 5: a) Dependence of the excitation energy (PBE/DZP) on the value of the CT threshold (a.u.), and b) dependence of the error in the excitation energy on the percentage of removed orbital transitions for the perylene dye I solvated by 42 methanol molecules. c) Dependence of the excitation energy (PBE/DZP) on the value of CT threshold, and d) dependence of error in the excitation energy on the percentage of removed orbital transitions for the perylene dye I adsorbed on  $\text{TiO}_2$  nanoparticle model.

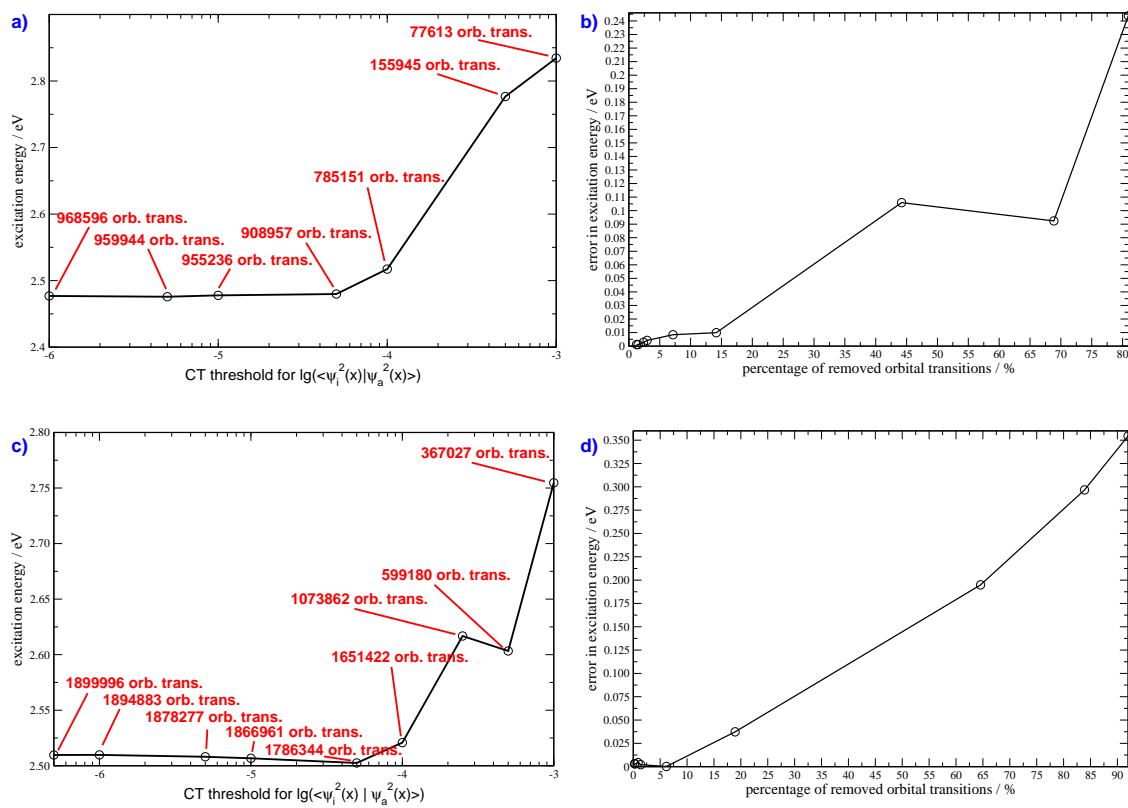


Figure 6: Structure of perylene dye II and dye II adsorbed on a  $\text{TiO}_2$  nanoparticle model (coordinates are taken from Ref. [18]).

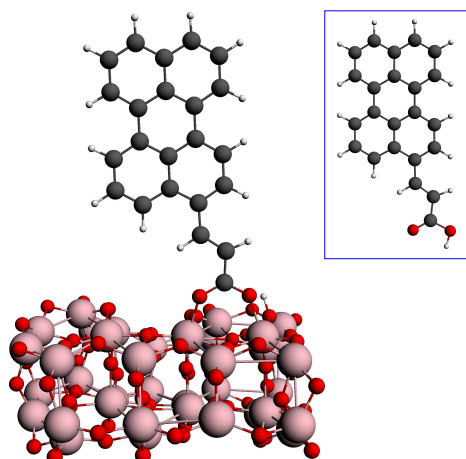


Figure 7: Isosurface plots of the HOMO and LUMO orbitals of the free perylene dye II and the dye II adsorbed on a TiO<sub>2</sub> nanoparticle model (isosurface value:  $\pm 0.03$ ).

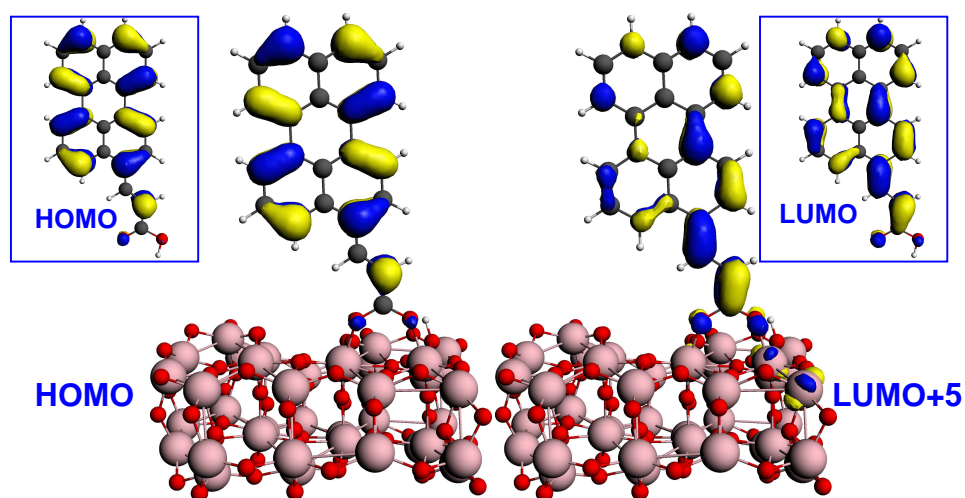


Figure 8: Dependence of the excitation energy on the value of CT threshold (a.u.) for the perylene dye II adsorbed on the  $\text{TiO}_2$  nanoparticle model [a)], and dependence of the error in the excitation energy on the percentage of removed orbital transitions [b)].

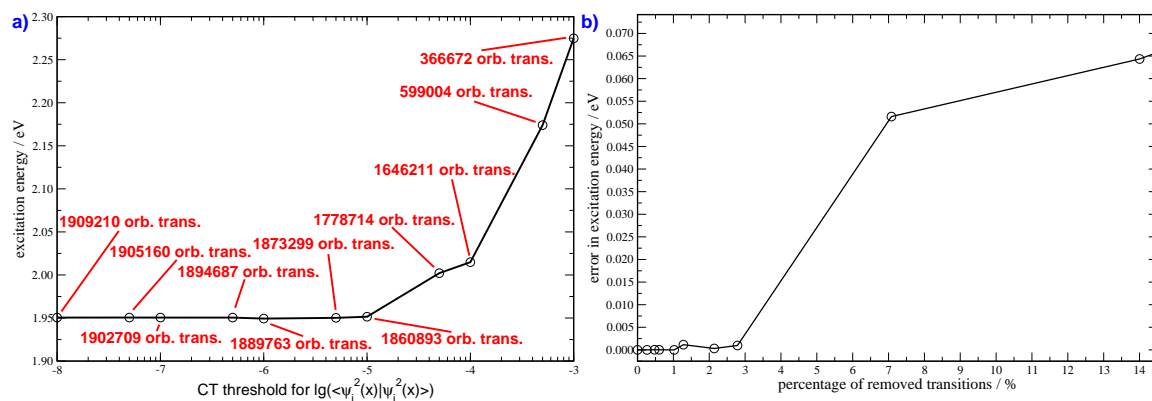
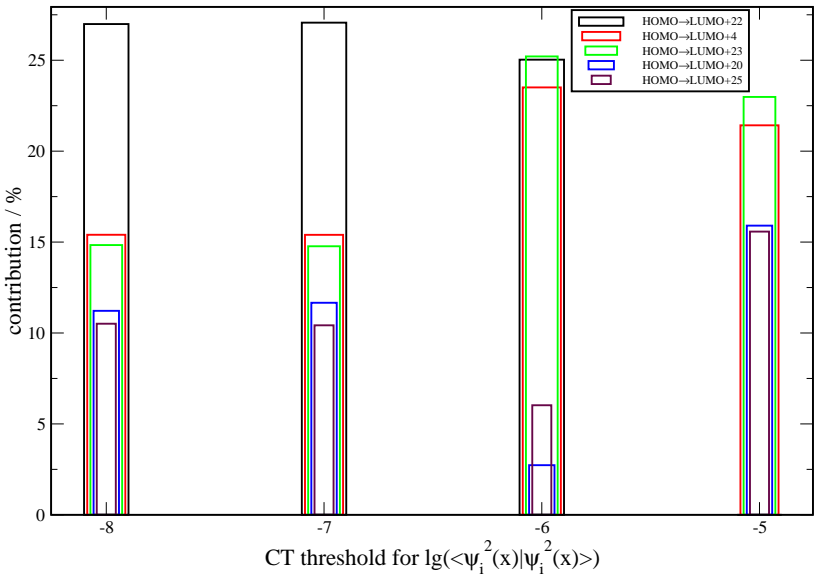


Figure 9: Orbital composition of excitation with highest contribution of HOMO→LUMO transition of perylene dye II in DSSC for different CT thresholds (a.u.).





## List of Tables

I	Excitation energies (in units of eV) dominated by HOMO→LUMO orbital transition of perylene dye I (see Fig. 3) calculated with different basis set and XC functionals. . . . .	41
II	HOMO→LUMO excitation energies (in units of eV) of the free perylene dye I and dye I adsorbed on a titanium dioxide nanoparticle model (env. = environment, conv. = conventional Davidson solver, sel. = selective Davidson solver). . . . .	42
III	HOMO→LUMO excitation energies (in units of eV) of the free perylene dye II and dye II adsorbed on a titanium dioxide nanoparticle model. . . .	43

Table I: Excitation energies (in units of eV) dominated by HOMO→LUMO orbital transition of perylene dye I (see Fig. 3) calculated with different basis set and XC functionals.

basis set	functional	PBE	SAOP	B3LYP
	DZ	2.67	2.67	2.92
	DZP	2.56	2.56	2.80
	TZP	2.53	2.53	2.76
	QZ4P	2.51	2.51	2.73

Table II: HOMO→LUMO excitation energies (in units of eV) of the free perylene dye I and dye I adsorbed on a titanium dioxide nanoparticle model (env. = environment, conv. = conventional Davidson solver, sel. = selective Davidson solver).

basis	functional	optimizer	env.	dye I	dye I on TiO <sub>2</sub>
DZP	PBE	conv.		2.56	2.51
DZP	PBE	sel.		2.56	2.51
DZP	PBE	conv.	COSMO	2.58	
DZP	PBE	sel.	COSMO	2.58	2.53
DZP	PBE	conv.	CSMRSP	2.49	
DZP	B3LYP	conv.		2.80	
DZP	B3LYP	conv.	CSMRSP	2.72	
6-31G*	B3LYP	conv.		2.87	
6-31G*	B3LYP [18]	conv.	C-PCM	2.79	2.73

Table III: HOMO→LUMO excitation energies (in units of eV) of the free perylene dye II and dye II adsorbed on a titanium dioxide nanoparticle model.

method	dye II	dye II on TiO <sub>2</sub>	shift
PBE/DZP (selective)	2.17	1.95	−0.22
B3LYP/6-31G*, C-PCM [18]	2.43	2.17	−0.26